

Article

Optimal Hyperspectral Characteristics Determination for Winter Wheat Yield Prediction

Yao Zhang ^{1,2,3}, Qiming Qin ^{1,2,3,*}, Huazhong Ren ^{1,2,3} , Yuanheng Sun ^{1,2,3}, Minzan Li ⁴, Tianyuan Zhang ^{1,2,3}  and Shilong Ren ^{1,2,3}

¹ Institute of Remote Sensing and Geographic Information System, School of Earth and Space Sciences, Peking University, Beijing 100871, China; zhycou@163.com (Y.Z.); renhuazhong@pku.edu.cn (H.R.); yhsun@pku.edu.cn (Y.S.); zhangtianyuan@pku.edu.cn (T.Z.); renshilong@pku.edu.cn (S.R.)

² Beijing Key Laboratory of Spatial Information Integration and 3S Application, Peking University, Beijing 100871, China

³ Mapping and Geo-information for Geographic Information Basic Softwares and Applications, Engineering Research Center of National Administration of Surveying, Beijing 100871, China

⁴ Key Laboratory of Modern Precision Agriculture System Integration Research, Ministry of Education, China Agricultural University, Beijing 100083, China; limz@cau.edu.cn

* Correspondence: qmqinpku@163.com; Tel.: +86-10-6275-1965

Received: 16 October 2018; Accepted: 10 December 2018; Published: 12 December 2018



Abstract: Crop growth in different periods influences the final yield. This study started from the agronomic mechanism of yield formation and aimed to extract useful spectral characteristics in different phenological phases, which could directly describe the final yield and dynamic contributions of different phases to the yield formation. Hyperspectral information of the winter wheat canopy was acquired during three important phases (jointing stage, heading stage, and grain-filling stage). An enhanced 2D correlation spectral analysis method modified by mutual information was proposed to identify the sensitive wavebands. The selected wavebands performed well with good mechanism interpretation and close correlation with important crop growth parameters and main physiological activities related to yield formation. The quantitative contribution proportions of plant growth in three phases to the final yield were estimated by determining the coefficients of partial least square models based on full spectral information. They were then used as single-phase weight factors to merge the selected wavebands. The support vector machine model based on the weighted spectral dataset performed well in yield prediction with satisfactory accuracy and robustness. This result would provide rapid and accurate guidance for agricultural production and would be valuable for the processing of hyperspectral remote sensing data.

Keywords: hyperspectral; winter wheat; yield; mutual information; 2D correlation spectra

1. Introduction

The world's population is projected to grow from 7 billion to approximately 9 billion by 2050. Although agricultural productivity has improved rapidly in recent decades, the requirements of a large population are difficult to meet due to natural resource shortage, climate change, and environmental pollution [1–3]. Therefore, ensuring food security has become the primary goal of global agricultural development. Accurately estimating crop growth status in different important phenological phases and predicting crop yield information are essential for effective food security warnings, guiding agricultural management, formulating agricultural policies, controlling the balance of food supply-demand, and ensuring sustainable agricultural development [4–6]. The use of remote sensing (RS) to monitor crop growth status and yield has considerably increased recently. RS allows the estimation and forecast of large zones on a regional or district scale [7], which are useful to public organizations and the

government. RS also allows the estimation and forecast of small areas on a field scale [8], thereby providing farm managers with precise agronomic strategies based on the expected yield potential [9].

There are two types of methods, which have been widely used to estimate crop yield with RS information. One is using the characteristic spectral information or its derivations, including spectral vegetation indices or spectral morphological parameters, that are correlated with elements representing crop growth status, namely, chlorophyll content and leaf area index (LAI) etc., to estimate crop yields [10–16]. Sid'ko et al. identified the chlorophyll potential indicators, which are the differences between the reflectance factor integrals in the 550 nm–730 nm wavelength range, and used the chlorophyll potential indices that varied with seasonal dynamics to construct yield estimation models for wheat, barley, and oat cultivars [15,16]. This sort of method is simple and could get acceptable results in particular conditions, which is highly dependent on specific cultivars, growth stages, or certain geographical regions [17]. These empirical statistical models have weak interannual and space expansibility due to the lack of an agronomic mechanism of yield formation at different growth stages. Another type of method is data assimilation, an approach that incorporates RS observations into crop simulation models based on mathematical descriptions of key physical, physiological processes of plant and environment changes [18,19]. Morel et al. [20,21] established the relationship of photosynthetically active radiation with the normalized difference vegetation index (NDVI) and with the light interception coefficient in the MOSICAS model and substituted the relationships into the model to achieve the yield inversion of sugar beet and sugar cane, respectively. Huang et al. [22–25] proposed multiple data assimilation frameworks that assimilated LAI, evapotranspiration (ET), or remote sensed reflectance into crop growth models or crop growth-radiative transfer model successively, which improves the reliability of regional-scale winter wheat yield estimation. However, in all the studies in which RS data are assimilated into crop models, there is one point that should be neglected is that not all the detailed parameters, namely, management practices, meteorological data, crop growth, or soil characteristics, can be acquired. The large size of these parameters and limited information available in situ cause problems, such as deviations in forecasting results and recurring instability.

Focusing on the limitations of both the methods mentioned above, a new type of crop yield forecasting method that considers both the agronomic mechanism of yield formation and the simplification of cumbersome growth parameters is urgently needed. Hyperspectral RS data, that contain numerous information representing the internal relations between radiation energy and the composition and structure of matters, provide unique opportunities for fast and reliable evaluation of characteristics associated both with various structural, biochemical, and physiological traits [26–28], which could be used as a promising approach for yield estimation. Hyperspectral data extend the spectral estimation ability by allowing the calculation of additional vegetation indices by narrow bands [29–31]. Aside from the current vegetation indexes (VIs) presented in the literature, hyperspectral signals can be used to calculate the complex combinations of all available wavelengths using traditional formulas or modern algorithms. Aguate et al. proved that prediction equations using 62 bands from hyperspectral data can lead to a better predictive performance for grain yield than what can be achieved using VIs [32]. Thorp et al. developed a genetic algorithm to mine narrow-band canopy reflectance and spectral derivative data for spectral features, and they identified less than 25 relevant spectral features, which further improved the accuracies of durum wheat yield estimation [33]. Therefore, groups of selected sensitive wavelengths exhibit extraordinary potential in crop yield estimation [34].

According to previous studies, to increase the accuracy and efficiency of crop yield prediction, some characteristic wavelength selection methods have been tested. However, low monitoring efficiency, insufficient data mining, and incomplete mechanism analysis limit the practical applications of existing achievements. Therefore, we should start from the perspective of yield formation and make full use of the hyperspectral characteristics of crops in different important phenological phases. The hyperspectral information can be used to directly estimate the dynamic accumulation of grain yield and further strengthen the mechanism analysis of wheat yield formation.

This study aimed to propose a new method for predicting crop yield via hyperspectral RS technology. To determine yield accumulation at different physiological phases, the canopy hyperspectral characteristics in each phase were investigated to trail the final yield information. The novelties of this study are listed as below: (1) an enhanced 2D correlation spectral method modified by mutual information (MI) theory was innovatively proposed. Using the final yield as the perturbation and target value, the most sensitive wavebands directly related to yield formation were determined to assess the change in final yield; (2) the contribution weights of different growth phenophases to the final yield accumulation was firstly quantified using the hyperspectral information; (3) the yield of winter wheat was predicted by the weighted characteristic spectral information combining the selected characteristic wavelengths and yield accumulation contribution weights, with sufficient mechanism interpretation and high accuracy. This study would provide a new concept for yield prediction using hyperspectral data and serve agricultural production with dynamic strategies.

2. Materials and Methods

2.1. Experiment Design

Field experiments were conducted in 2017, at an agricultural region in Hengshui City (115°10′–116°34′E, 37°03′–38°23′N) of Hebei Province, China. The region is part of the Huang-Huai-Hai Plain of China, which is an alluvial plain of the Yellow River, Huaihe River, and Haihe River [35]. In this region, winter wheat is the primary crop, and the main crop planting pattern is rotation of winter wheat and summer maize [36,37]. For winter wheat, the developmental period occurs from early October to early June of the next year. Field data measurement was conducted on the winter wheat with a single genotype during the three key phenological phases: Jointing stage (12 April), heading stage (5 May), and grain-filling stage (31 May) of winter wheat. The relatively homogeneous fields with a size larger than 1 km² were selected. A total of 21 fields were examined. In each field, five plots were deployed diagonally with a distance longer than 50 m to each other as shown in Figure 1. Besides, all points are further than 50 m from the edge of the field. Thus, 105 plots were selected for all experiments (hyperspectral measurement in three phenological phases and final yield estimation in the harvest time). In addition, a Global Positioning System (GPS, Trimble GeoExplorer 6000 Series GeoXH, Trimble Navigation, Ltd., Sunnyvale, CA, USA) was used to record the coordinates so that the same corresponding positions could be accurately located at different growth stages.

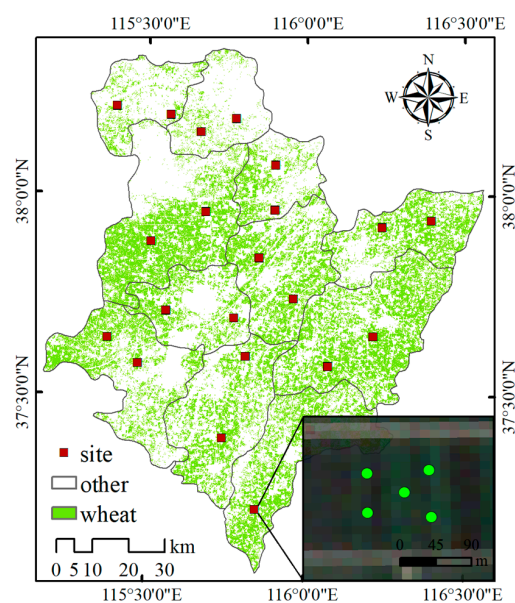


Figure 1. Experiment locations.

2.2. Spectra Measurement

The spectral reflectance of winter wheat canopy was obtained at three phenological phases by an ASD FieldSpec FR spectroradiometer (Analytical Spectral Devices Inc., Boulder, CO, USA), covering the spectral range from 350 nm to 2500 nm with a sampling interval of 1 nm. To calibrate the ASD instrument before canopy reflectance measurements, a spectralon white reference panel (Labsphere, Sutton, NH, USA) was used to calculate the baseline reflectance of the calibration panel. Under clear sky conditions between 10:00 and 14:00 Beijing time, reflectance values were obtained at 1.0 m above the canopy. In each observation, to reduce the possible effects of sky and field conditions, five measurements were conducted randomly and averaged to derive the representative reflectance spectra for each plot. Vegetation and panel radiance measurements were taken as the average of 20 scans at an optimized integration time, with a dark current correction for each spectrometry measurement.

2.3. Winter Wheat Yield Calculation

All the ears from plant samples, which were collected from 1 m² at each sample plot, were heated to 105 °C and oven dried at 80 °C until they reached a constant weight in the laboratory. Then, the dried grains were manually collected from the ears and the final dry weight of grains was recorded with unit of g. The yield of this plot was calculated by dividing the recorded grain weight by 1 m². Additionally, the unit was then converted from g/m² to t/ha. Then, a total of 105 yield data of winter wheat were acquired from 21 fields. After preprocessing using the box-plot method, six abnormal yield values in the range of 5.344 t/ha–5.973 t/ha were eliminated. Then, the 99 sample points with yields in the range of 6.421 t/ha–9.418 t/ha were obtained.

2.4. Data Analysis

2.4.1. 2D Correlation Spectrum

Compared with traditional 1D spectroscopy analysis, 2D correlation spectroscopy analysis shows greater advantages, such as improving the spectral resolution, solving the problems of overlapping, and determining the attribution of certain puzzle peaks. The system of 2D correlation spectroscopy analysis generates dynamic changes induced by external disturbances; thus, the congested or overlapped peaks that are covered in the 1D spectral information will extend and display visibly in the third dimensional direction [38]. This method can considerably enhance the spectra identification capability [39].

In this study, the dynamic spectrum of the winter wheat canopy was obtained by inducing the final yield as the perturbation factor. 2D correlation analysis was conducted using a self-developed software.

The dynamic spectra, $\tilde{y}(v, t)$, used in 2D correlation spectroscopy analysis are defined in Equation (1) [40]:

$$\tilde{y}(v, t) = \begin{cases} y(v, t) - \bar{y}(v) & T_{min} < t < T_{max} \\ 0 & \text{else} \end{cases} \quad (1)$$

where $\bar{y}(v)$ is the reference spectrum of the system, which is usually the average of the observations, and t is the outer interference. In the presence of outer interference, the dynamic spectra are calculated by subtracting the reference spectrum from the original spectrum. In the absence of outer interference, the value is zero.

The intensity, $X(v_1, v_2)$, of 2D correlation spectroscopy was obtained by analyzing the correlation between the corresponding variations of $\tilde{y}(v, t)$ caused by two independent variables, v_1 and v_2 , respectively. The formula for the intensity is shown as Equation (2) [38]:

$$X(v_1, v_2) = \varnothing(v_1, v_2) + i\psi(v_1, v_2) \quad (2)$$

where $\varnothing(v_1, v_2)$ is the intensity of 2D correlation synchronization, which represents the overall similarity or coincidental degree of the intensity changes caused by two independent optical variables

with an external disturbance of t . The synchronous correlation spectrum is symmetric with the principal diagonal showing the synergy between two dynamic spectrum signals. The peaks at the diagonal were called auto-peaks and obtained via the autocorrelation of dynamic spectra [41]. The 2D asynchronization correlation intensity, $\psi(v_1, v_2)$, represents the out-of-phase or difference of the intensity variance.

2.4.2. MI

MI is a quantitative index of the amount of information in one variable relative to the information in other variables. MI theory can effectively eliminate the irrelevant information to the target components (y) from the variable information (x). Thus, MI is expressed as Equation (3) [42,43]:

$$MI(x, y) = \iint dx dy \mu(x, y) \log \frac{\mu(x, y)}{\mu_x(x) \mu_y(y)} \quad (3)$$

where x represents the spectral information of each waveband; y represents the final yield data; $\mu(x, y)$ is the joint density, and $\mu_x(x)$ and $\mu_y(y)$ are the edge densities.

The nonlinear relationship is ubiquitous between the spectral information and the corresponding material concentration [44–46]. MI technology can consider both linear and nonlinear relationships between variables, and it outperforms other correlation analysis methods.

2.4.3. MI-Enhanced 2D Correlation Spectrum

Considering the outstanding advantages of 2D correlation spectrum analysis and MI in feature selection, this research proposed an innovative feature selection method called MI-enhanced 2D correlation spectrum technology by combining the two abovementioned methods to deeply explore the internal relationship between variables and extract more detailed information related to winter wheat yield from the canopy hyperspectral data. The steps of the wavelength selection process are as follows:

1. Initialization. This step involves inputting the original spectral reflectance with the corresponding yield data and rearranging the input dataset to ensure the constant increase in the perturbation variable.
2. Calculating and normalizing MI. In this step, the MI value between the yield value and reflectance of each wavelength is calculated with Equation (3). The acquired MI value is then normalized from 0 to 1 via Equation (4):

$$x_i' = (x_i - x_{min}) / (x_{max} - x_{min}) \quad (4)$$

where x_i and x_i' are the MI and normalized MI at wavelength i , respectively; x_{min} and x_{max} are the minimum and maximum MI values, respectively.

3. Data fusion. The MI-merged spectral information, which enhances the ability of the original spectral expression in the relationship with external disturbances, is constructed in this step through Equation (5):

$$A_i = w_i \times x_i' \quad (5)$$

where A_i is the MI-merged spectral information at wavelength i , and w_i is the original spectral information at wavelength i .

4. Data preprocessing. To reduce the effect of data dispersion on the display of 2D correlation spectra, the spectral data should be standardized as shown in Equation (6):

$$SA_i = \frac{A_i - \bar{A}_i}{\sqrt{std(A_i)}} \quad (6)$$

5. 2D correlation. The standardized MI-merged spectral information is then used for the 2D correlation analysis mentioned in Section 2.4.1.

6. Peaks' selection criteria. The peaks on the principal diagonal in the enhanced synchronous correlation spectrum represented the susceptibility of vibrations of the certain functional group with increasing yield. The wavelengths of some specific peaks can be selected as the sensitive wavebands. In order to make the best of the characteristics of the crop spectral information and further decrease the redundancy of the selected wavelengths, the criteria of peaks' selection on the diagonal of the *MI*-enhanced 2D correlation spectrum is set as below: The selected peaks should have a prominence of at least A , and the distance between the selected peaks should be larger than B . A and B could be calculated through Equations (7) and (8):

$$A = \frac{\max(R_\lambda)}{B} \quad \lambda \in [350, \text{end}] \quad (7)$$

$$B = \frac{R_{\text{red-edge}}}{\max(R_\delta)} \quad \delta \in [350, R_{\text{red}}] \quad (8)$$

where R_λ is the reflectance in the range from 350 nm to the end, $R_{\text{red-edge}}$ is the reflectance at the red-edge position, and R_δ is the reflectance in the range from 350 nm to the reflectance valley in the red region.

2.4.4. Contribution Ratio Determination

This study adopted the entire wavelength information from 350 nm to 900 nm for the three periods to establish partial least square (PLS) models for the final yield estimation. The determination coefficients of the three models were used to calculate the quantitative contribution ratios through Equation (9):

$$\omega_i = \frac{R_i}{\sum_{i=1}^3 R_i} \quad (9)$$

In Equation (9), ω_i represents the contribution ratio of the full spectral information to the winter wheat yield at a certain stage, and R_i is the determination coefficient of the i th period.

2.4.5. Weighted Spectral Information Calculation

- Weighted characteristic spectral information calculation

After obtaining the contribution ratios of the three phenological phases to the final yield of winter wheat, the weighted characteristic spectral information was constructed by Equation (10) based on the sensitive wavelengths selected through enhanced 2D correlation spectral analysis:

$$R'_i = \omega_i \times R_i \quad (10)$$

where ω_i is the weight of the i th period. R_i and R'_i are the original and weighted reflectance in the i th period, respectively.

The three groups of the weighted reflectance calculated by the characteristic wavelengths and final yield contribution ratios of the three periods were used for yield prediction.

- Weighted full-spectral information calculation

The weighted full-spectral information based on the obtained contribution ratios and full-spectral information was constructed by Equation (11):

$$R'_n = \omega_1 \times R_{1n} + \omega_2 \times R_{2n} + \omega_3 \times R_{3n} \quad (11)$$

where ω_1 is the weight of the jointing period, ω_2 is the weight of the heading period, and ω_3 is the weight of the grain-filling period. R_{1n} , R_{2n} , and R_{3n} are the original reflectance of n th wavelength in the joint, heading, and grain-filling stage. R'_n is the weighted reflectance of n th wavelength.

2.4.6. Support Vector Machine Regression

Support vector machine (SVM) is a universal machine learning algorithms invented by Cortes and Vapnik [47]. It has many unique advantages in classification and regression analysis, such as solving problems from small samples and converting the nonlinear relations of the training data into a linear function in a higher dimensional feature space [48]. SVM is built based on the VC-dimension of statistical learning theory and the minimum structural risk principle [49]. Important parameters include the kernel function and the cost loss function [50].

Considering the advantages of SVM and characteristics of the dataset in this study, the SVM regression model was selected as the winter wheat yield prediction model. The type of kernel function is the radial basis function. The optimal values of the penalty parameter, C , and the kernel function parameter, g , were determined by the cross validation method using libsvm 2.89 [51].

3. Results

3.1. Characteristic Analysis of VIS/NIR Spectra

In the entire range of 350 nm–2500 nm, the spectral information in the visible and NIR-infrared regions was highly correlated with the important crop growth parameters and main physiological activities of plants, which were all related to the final yield accumulation. Moreover, the spectral information in this band could also be acquired by most UAV hyperspectral platforms, which provides a possibility of future application in winter wheat yield prediction at a regional scale. Thus, the spectral information in the range of 350 nm–900 nm was used for analysis. Figure 2 shows the original hyperspectral reflectance of all samples with gray color and the averaged hyperspectral reflectance with black color of the winter wheat canopy at the three physiological phenophases.

The change tendency of the canopy hyperspectral reflectance at the three periods was basically the same. In the visible spectral region of 350 nm–690 nm, the overall reflectance was low because the majority of incident light was absorbed by chlorophyll and carotenoids during photosynthesis. A green peak was observed at approximately 550 nm, which was caused by the strong absorption by the pigments in the blue and red spectral region and weak absorption near 550 nm [52]. The reflectance increased sharply at around 690 nm–750 nm, reflecting the red-edge characteristic of green plants. Then, the reflectance remained at a high and stable value. From the jointing stage to the heading stage, the photosynthesis intensity of the whole wheat population continuously increased with the amount of photosynthetic parameters increasing and leaf area expanding [53]. Meanwhile, the absorption in the visible light region was gradually enhanced, and the reflectance decreased [52–54]. During the grain-filling period, most parts of the plants start to turn yellow and less biochemical contents for photosynthesis left in the plant [53,55]. Thus, the reflectance characteristics of green plants in the visible range were almost absent.

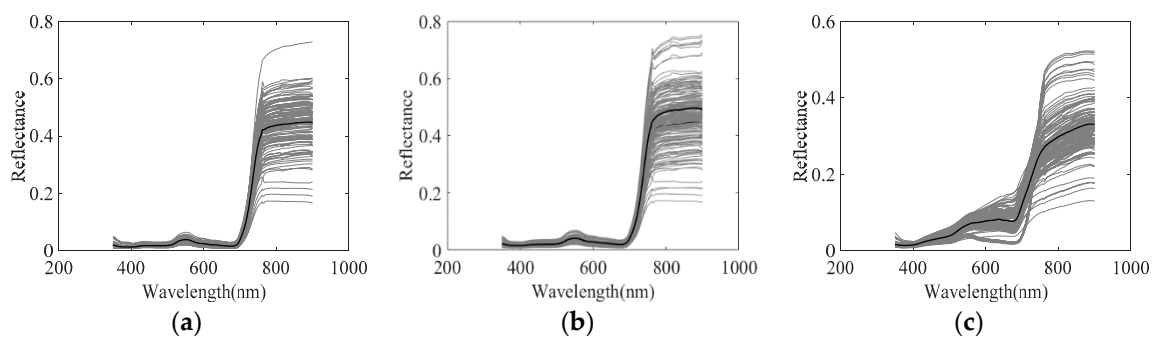


Figure 2. Spectral reflectance of the winter wheat canopy: (a) Jointing stage, (b) heading stage, and (c) grain-filling stage.

3.2. Traditional 2D Correlation Spectroscopy at the Three Phenological Phases

The traditional 2D correlation spectra at the three phenological phases are shown in Figure 3. The figure for the heading stage shows more details than the two other stages, indicating that the physiological activities related to yield formation in the heading stage were stronger than those in the other stages. However, only one or two wavelengths could be selected in the jointing stage and grain-filling stage based on the peaks in principal diagonals, e.g., 552 nm and 694 nm for the jointing stage and 735 nm for the grain-filling stage. Thus, it is insufficient to only use the traditional 2D correlation spectral analysis to extract all characteristic spectra reflecting yield information from canopy hyperspectral information in different growth stages. Since the relationship between the canopy spectral characteristics in three phases with the final yield is complex, some deep exploration toward the hyperspectral data should be done.

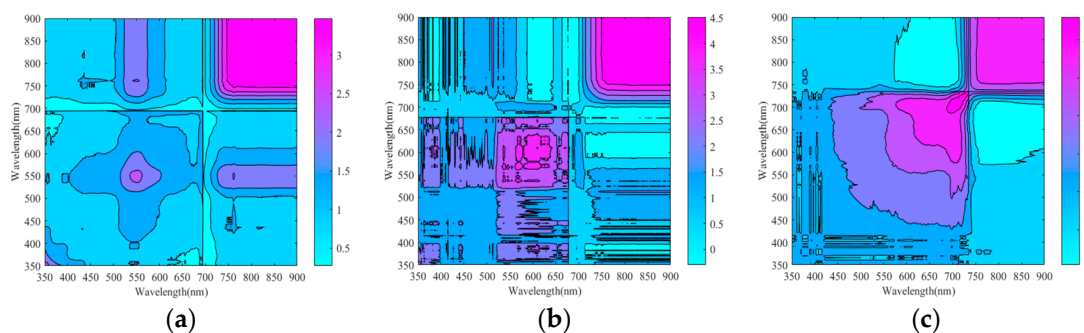


Figure 3. Contour map of synchronous traditional 2D correlation spectra at 350 nm–900 nm: (a) Jointing stage, (b) heading stage, and (c) grain-filling stage.

3.3. Sensitive Waveband Selection Based on the Enhanced 2D Correlation Spectroscopy Method by MI

Considering the limitation of the traditional 2D correlation spectral method, this research calculated *MI* values between the canopy spectral information at the three phenophases and the yield data, respectively (shown in Figure 4), and introduced it to the conducted *MI*-enhanced 2D correlation spectral analysis to directly acquire the sensitive wavelengths representing the final yield in three phenological phases.

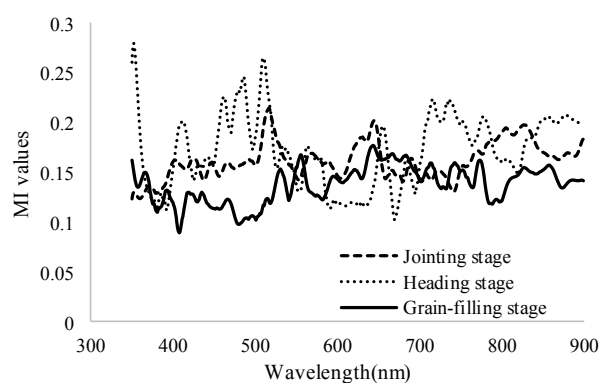


Figure 4. *MI* curves in the range of 350 nm–900 nm.

3.3.1. 2D Spectral Characteristic Analysis of Winter Wheat Canopy during the Jointing Period

Figure 5a,b show the contour of the winter wheat canopy synchronous 2D correlation spectra at 350 nm–900 nm and the principal diagonal. According to the peak selection criteria, seven auto-correlational peaks were observed around 426 nm, 518 nm, 565 nm, 645 nm, 731 nm, 806 nm, and 828 nm, which illustrated that the spectral intensities of these wavelengths fluctuated with the outer interference. The seven wavelengths were highly sensitive to the variance in final yield.

According to the published literature, the peak at 426 nm could be caused by the reaction of chlorophyll a, carotenoids, and flavins [56,57]. The peak at 645 nm was related to chlorophyll b [58]. The peak at 518 nm was the sensitive waveband of lutein and lutein-chlorophyll b complex [59,60], and 565 nm and 731 nm were the nitrogen-related wavelengths [61]. The sensitive wavelength reflecting photosynthetic bacteria appeared at 806 nm [62]. In redox reactions, 828 nm was the sensitive wavelength of the oxidation process in redox reactions [63]. Besides the chemical parameters mentioned above, some selected sensitive wavelengths were related to biophysical parameters, such as LAI. Four wavelengths (426 nm, 518 nm, 565 nm, and 645 nm) were in the range of LAI sensitive wavebands (400 nm–700 nm) [64]. LAI was used to calculate the photosynthetically active absorbed radiation (PAR_A) [65], which is closely related to the canopy photosynthesis [53].

The selected wavelengths were sensitive to the chemical and biophysical parameters, which determined the photosynthetic capacity and efficiency [66]. There is strong evidence that increasing photosynthesis will increase crop yields, as demonstrated by the effects on yield of CO_2 -enrichment experiments [67]. Hence, the selected sensitive wavelengths were closely related to photosynthesis and could further reflect the winter wheat yield in this period.

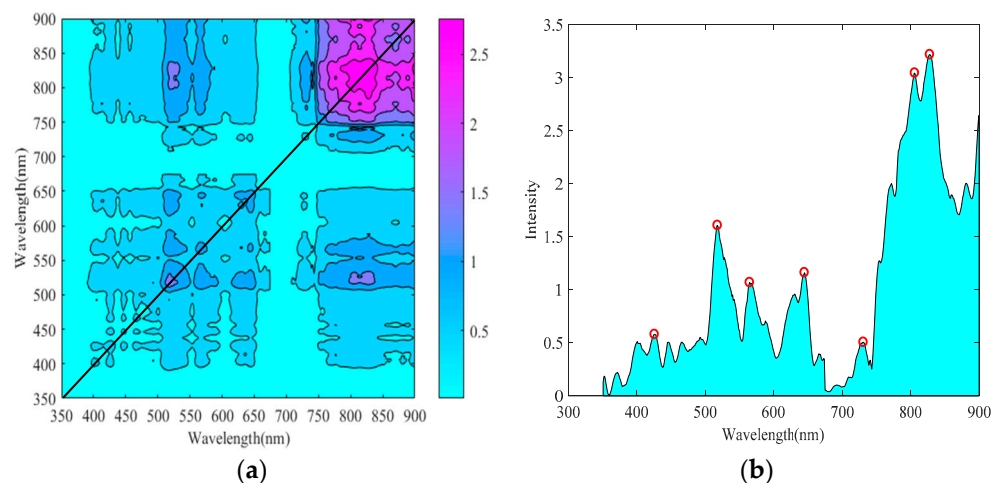


Figure 5. 2D correlation spectra of the winter wheat canopy for the jointing period: (a) Synchronous 2D spectra contour map; (b) diagonal of the synchronous contour map.

After observing the synchronous 2D correlation spectra and analyzing the mechanism of the attribution of the selected wavelengths, the characteristic spectral information for the winter wheat canopy to yield accumulation during the jointing stage was obtained. This information could further explain the main physiological process of yield formation at this stage.

3.3.2. 2D Spectral Characteristic Analysis of the Winter Wheat Canopy during the Heading Period

Figure 6a,b show the synchronous 2D correlation spectra and the principal diagonal graph during the heading period. The figures for this period have more details compared with those for the jointing stage. Thirteen featured wavelengths (385 nm, 410 nm, 442 nm, 463 nm, 485 nm, 510 nm, 536 nm, 564 nm, 657 nm, 677 nm, 755 nm, 779 nm, and 878 nm) were sensitive to the variance in yield interference and were selected for this period.

Among the 13 selected wavelengths, the wavelengths of 385 nm, 485 nm, and 878 nm were related to the photosynthetic bacteria [62], and 10 wavelengths (385 nm, 410 nm, 442 nm, 463 nm, 485 nm, 510 nm, 536 nm, 564 nm, 657 nm, and 677 nm) were sensitive to LAI [64]. The wavelengths of 442 nm, 564 nm, 657 nm, and 677 nm were in the range of chlorophyll-sensitive wavebands [59]. The wavelength of 442 nm was also sensitive to potassium, which plays an important role in photosynthesis, such as in stomatal regulation, activation of photosynthetic enzymes, and transportation of assimilates [43]. The wavelength of 564 nm was related to phosphorus, which directly participates in the assimilation

and photosynthetic phosphorylation of photosynthesis. Phosphorus is also an important element of adenosine triphosphate and NADPH [68]. The wavelengths of 410 nm and 755 nm were linked to nitrogen, which influences photosynthesis dramatically [69]. On the one hand, nitrogen increases the number of chloroplasts, with the surface area and volume of chloroplasts increasing per unit volume of leaves, resulting in the expansion of the exchange interface between chloroplasts and the external energy and substances. On the other hand, nitrogen changes the structure of chloroplast grana by increasing the grana diameter, number of stacks, and thickness of thylakoids. Therefore, the photosynthetic pigments (chlorophyll a, chlorophyll b, and carotenoids) on the thylakoid membrane also increase, strengthening the photosynthetic capacity of the chloroplasts. Moreover, the wavebands within 710 nm–790 nm had high reflectivity due to the presence of cellulose and other structural carbohydrates [70,71]. The wavelength of 463 nm was sensitive to chlorophyll b, carotenoids, and flavins [56], whereas that of 510 nm was related to phototropins [72,73]. These compounds are the basic elements for photosynthesis and are crucial for vigorous plant growth [74].

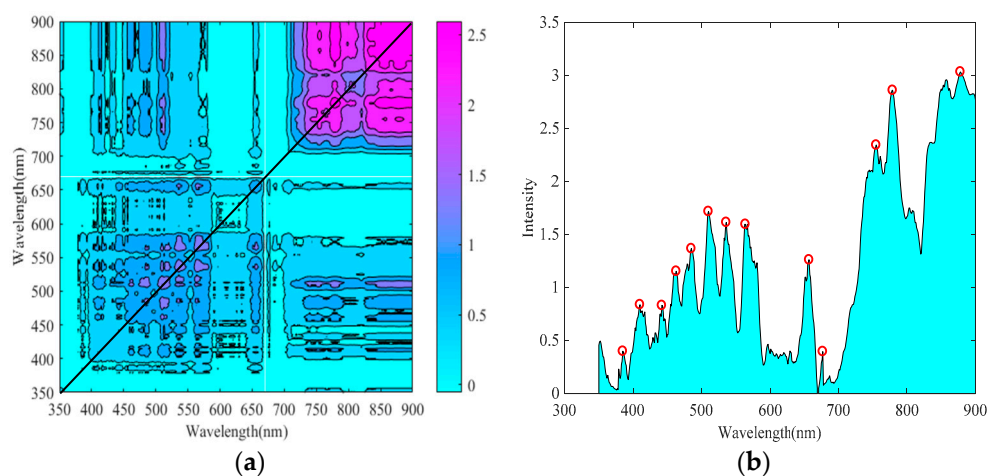


Figure 6. 2D correlation spectra of the winter wheat canopy for the heading period: (a) Synchronous 2D spectra contour map; (b) diagonal of synchronous contour map.

The analysis of the 2D synchronous correlational spectra revealed intensive physiological activity at the heading stage and identified additional characteristic spectral information of winter wheat. In addition to the sensitive wavelengths associated with chlorophyll and LAI, sensitive wavelengths related to nitrogen, phosphorus, and potassium were also identified. These elements are indispensable for crop photosynthesis. These findings indicated that photosynthesis was quite active, resulting in high crop productivities during this period [66]. Therefore, enhanced 2D correlation spectroscopy could effectively extract key spectral information reflecting crop growth and intensity of physiological activities related to the final yield at this stage.

3.3.3. 2D Spectral Characteristic Analysis of the Winter Wheat Canopy during the Grain-Filling Period

Nine wavelengths (531 nm, 556 nm, 644 nm, 668 nm, 713 nm, 755 nm, 774 nm, 828 nm, and 858 nm) were selected for the grain-filling period to predict the winter wheat final yield based on previous criteria (Figure 7). All selected wavelengths shifted to the long wavelength direction (Figure 7b). Among the selected wavelengths, 531 nm, 556 nm, 713 nm, 755 nm, and 858 nm were correlated with nitrogen content and nitrogen accumulative amount, which were the main factors for the final yield [55,61,69,75]. The two chlorophyll-related wavelengths were 644 nm and 668 nm [58,68,76]. The sensitive wavelength reflecting photosynthetic bacteria was 858 nm during this period [62]. The wavelength of 774 nm was correlated with oxygen, water, and carbohydrates [58,70,71]. Similar to the jointing period, 828 nm was the sensitive wavelength for the oxidation process in redox reactions [63]. Four wavelengths, including 531 nm, 556 nm, 644 nm, and 668 nm, were related

to LAI [64]. These results illustrated that there was less characteristic spectral information representing a typical green plant and more information about the nutrients of winter wheat at this stage compared with the other two stages.

On the basis of the analysis of the synchronous spectrogram and the principal diagonal graph, the spectral information at the grain-filling period could not reflect the typical spectral characteristics of green plants. During this stage, most parts of the canopy became yellow. As a result, the photosynthesis intensity began to weaken and only maintained basic activity to ensure sufficient energy for nutrient transportation. Furthermore, additional nitrogen-related wavelengths were chosen because in this period, nitrogen became more than an auxiliary for photosynthesis. It is translocated rapidly from other plant parts to the grain as a major substance for nutrient transport during yield formation [55].

The comprehensive analysis of the *MI*-enhanced 2D correlation spectral features of the winter wheat canopy at the three physiological phenophases showed that the sensitive wavelengths could represent the important crop growth parameters and corresponding physiological activities, which were related to the final crop yield at different phases. The proposed innovative *MI*-modified 2D correlation spectral analysis could effectively enhance the interference from the outer disturbance (final yield) to the original spectra and increase the interpretation ability of the original 2D correlation spectral method.

Except for the featured wavelength selection, the enhanced 2D correlation spectral technology could also be used to assess the physiological activity intensity related to yield formation during different phenological phases. The synchronous spectrum at the heading stage displayed the most useful sensitive wavelengths and details, followed sequentially by the grain-filling stage and jointing stage (Figures 5–7).

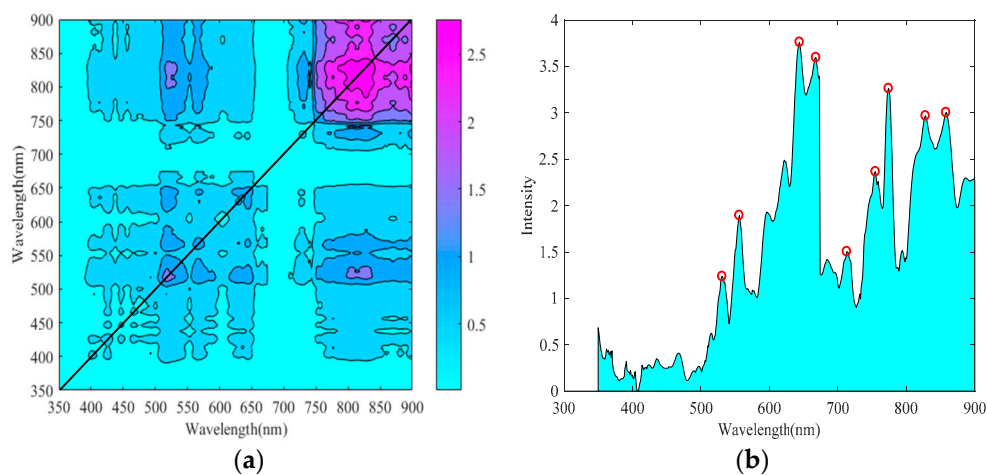


Figure 7. 2D correlation spectra of the winter wheat canopy for the grain-filling period: (a) Synchronous 2D spectra contour map; (b) diagonal of synchronous contour map.

3.4. Contribution Ratio Determination to Winter Wheat Yield Accumulation

The comprehensive analysis of the results of the feature selection using the enhanced 2D correlation spectrum indicated that the photosynthesis intensity increased from the jointing stage to the heading period with increasing photosynthetic pigment contents and canopy structure. The photosynthesis intensity decreased during the grain-filling period because the leaves turned yellow gradually. Except for the physiological activities related to photosynthesis, nutrient transport during the grain-filling period became more pronounced than that during the two other stages. After Equation (9), the quantitative contribution ratios of the different periods to the final yield of winter wheat were determined, which are shown in Figure 8.

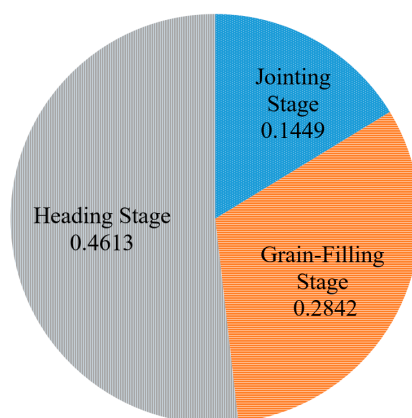


Figure 8. Contribution ratios of the three phenological phases.

Figure 8 is the pie chart of the contribution ratios of the three phenological phases, which shows that the heading period had the highest contribution ratio, followed by the grain-filling stage and then the jointing stage. The structure of the canopy and chemical parameters content of winter wheat increased dramatically from the jointing stage to the heading stage, thereby resulting in increased photosynthetic intensity. Furthermore, although the plant parts turned yellow gradually from the heading stage to the grain-filling stage, nutrient transport was enhanced apparently, which is a major factor in yield accumulation. The calculated contribution ratios based on full spectral information verified the results of enhanced 2D correlation spectral analysis.

3.5. Winter Wheat Yield Prediction Modeling and Analysis

To further verify the robustness and predictive ability of weighted characteristic spectral information, two mixed datasets, one containing the weighted characteristic spectral information and another one containing the weighted full-spectral information, of winter wheat canopy was created. Then, the SVM regression models based on the weighted characteristic wavelengths calculated through Equation (10) and weighted full-spectral information calculated through Equation (11) for the winter wheat yield were established, respectively. For each model, the samples were divided into two groups: 75 samples were under the calibration group, and the remaining 24 samples constituted the validation group.

The 1:1 relationship diagrams were drawn between the prediction and observation groups to demonstrate the reliability and consistency of the two models. Results are shown in Figures 9 and 10.

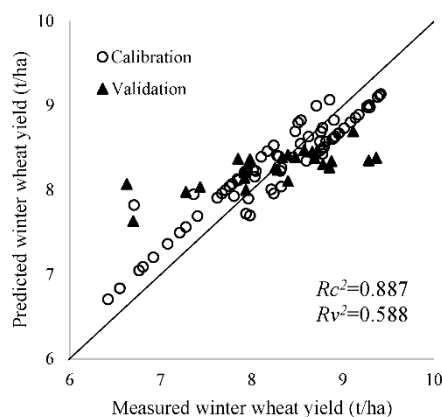


Figure 9. Calibration and validation of winter wheat yield prediction based on the weighted full-spectrum information.

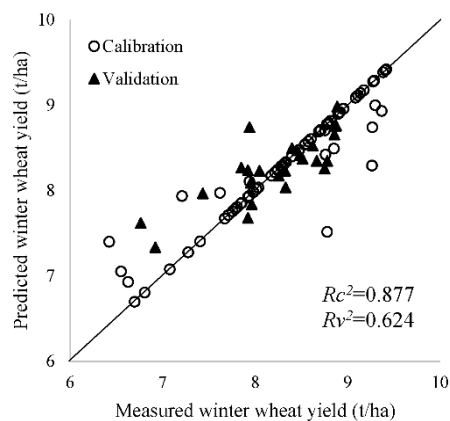


Figure 10. Calibration and validation of winter wheat yield prediction based on the weighted characteristic spectral information.

Figure 9 shows the results of the SVM model based on the weighted full spectra. The calibration R^2 of the model reached 0.887, and RMSEC was 0.289 t/ha; the validation R^2 reached 0.588, and RMSEP was 0.559 t/ha. Figure 10 shows the results of the SVM model based on the weighted characteristic spectra. The calibration R^2 of the model reached 0.877, and RMSEC was 0.27 t/ha; the validation R^2 reached 0.624, and RMSEP was 0.353 t/ha.

Both models produced acceptable accuracies, which proved the feasibility of winter wheat yield prediction using the spectral information of the plant canopy from different phenological phases. Except that the calibration R^2 of weighted full-spectra model is slightly higher than that of the characteristic spectra model, other indexes, including validation R^2 , RMSEC, and RMSEP, are all lower than that from the characteristic spectra model. In addition, when the actual yield was under 8 t/ha, the predicted values using the SVM model based on the weighted full spectral information were all higher than the measured yield. Therefore, the model established by the weighted selected wavelengths exhibited overall better performance. This result demonstrated that the selected sensitive wavebands using the *MI*-enhanced 2D correlation spectral analysis method could represent the useful information related to the yield formation and reduce the redundancy of full spectral information effectively, and the combination of the selected wavebands and the contribution ratios of the three key phenological phases could predict the winter wheat yield with good robustness and veracity.

4. Discussion

Prior work has documented the potential of selected sensitive wavelengths from hyperspectral information in crop yield estimation. Some characteristic wavelength selection methods have been used to increase the accuracy and efficiency of crop yield prediction. However, there have been few reports about the comprehensive interpretation of the relationships between the selected wavelengths and the important crop growth parameters, main physiological activities, and final yield formation. The lack of agricultural mechanism analysis decreases the universality and predictive ability of the established models.

In this study, we proposed a winter wheat yield prediction method, which is based on an innovative *MI*-enhanced 2D correlation spectral technology. This method was used to extract the spectral features of the plant canopy reflectance in the range of 350 nm–900 nm. The selected wavelengths were correlated with the important crop growth parameters and corresponding physiological activities of the plant, which were proved by the published literature [53–65,68–76]. These crop growth parameters and physiological activities were highly correlated with the final yield formation [55,66,67]. On these basis, these findings provided the mechanism analysis about the internal relationship between the selected wavelengths and crop yield and laid a theoretical basis for future assessments on the selected wavelengths for winter wheat yield prediction.

Moreover, the SVM prediction model that was established by the weighted characteristic spectral information outperformed the model based on weighted full-spectral information and obtained a satisfactory result in winter wheat yield prediction. Besides, compared with similar studies about the plant yield prediction using the extracted spectral features, this study also obtained slightly higher accuracies [33,34]. These results indicated that the integration of the selected wavelengths and contribution ratios could effectively improve the predictive ability of the winter wheat yield and further confirmed the effectiveness and superiority of the proposed *MI*-enhanced 2D correlation spectral analysis in feature extraction for winter wheat yield prediction. Our study provided a new framework for yield prediction using the canopy spectroscopy and the results may serve farm managers with dynamic production strategies on the basis of the expected yield.

However, some limitations should be worth noting. The proposed method in this study is only applied on winter wheat with a single genotype and grown in limited year and regions. The use of this method on more kinds of crops with different genotypes or grown under various suboptimal conditions (in stress conditions, insufficient nutrition status), in different locations and years needs to be validated. In addition, the impact from phenology should also be considered in future works. More in-depth research should be conducted to verify the reliability of the proposed *MI*-enhanced 2D correlation spectral analysis method and make it applicable in the multiple RS platforms.

5. Conclusions

To propose an effective and accurate method for the prediction of winter wheat yield, ground-based canopy hyperspectral information was used as the data source. Through the *MI*-enhanced 2D correlation spectral analysis with the corresponding final yield of winter wheat as the perturbation factor, the sensitive wavebands of yield at the three periods were obtained. The hyperspectral information at the three periods was used to determine the quantified yield contribution ratios, which were used as the weights of the different growth periods to calculate the characteristic spectra based on the selected sensitive wavelengths. The winter wheat yield prediction model was established by using the weighted characteristic spectral data of the plant canopy. This research attempted to forecast the winter wheat yield at specific growth stages precisely and rapidly. The main conclusions were drawn from this study:

- (1) After wavelength selection using the proposed *MI*-enhanced 2D correlation spectral analysis, three groups of wavelengths at the different growing periods were determined as the winter wheat yield sensitive wavebands. Spectral mechanism analysis revealed that such wavelengths correlated with the important crop growth parameters and represented the physiological activities, which were directly or closely related to the final yield formation. Results proved that the *MI*-enhanced method could effectively extract the sensitive wavelengths of plant physiological characteristics in yield formation.
- (2) The winter wheat yield contribution ratios were calculated from the hyperspectral information in the range of 350 nm–900 nm. The heading period had the highest contribution ratio, followed by the grain-filling stage and then the jointing stage. These results coincided with the activity levels in the enhanced 2D correlation spectrum for the three periods. Thus, the proposed *MI*-enhanced 2D correlation spectral analysis method demonstrated potential in assessing dynamic variance in winter wheat yield formation for each growth period.
- (3) Three groups of comprehensive weighted characteristic spectral information for the different periods were obtained combining the selected wavelengths and contribution ratios. Such information was used as the input data to establish the SVM prediction model. The calibration R^2 of the model reached 0.877, and RMSEC was 0.27 t/ha; the validation R^2 reached 0.624, and RMSEP was 0.353 t/ha. The model performed well in yield prediction with satisfactory accuracy and robustness. Its performance verified the effectiveness of the selected wavelengths and indicated that the winter wheat yield could be predicted using the plant canopy spectral information at different periods.

Author Contributions: Conceptualization, Y.Z. and H.R.; Methodology, Y.Z. and T.Z.; Software, Y.Z.; Validation, Y.Z. and S.R.; Writing-Original Draft Preparation, Y.Z.; Writing-Review & Editing, Y.Z., M.L. and T.Z.; Visualization, Y.Z. and Y.S.; Project Administration, Y.Z. and Q.Q.; Funding Acquisition, Q.Q.

Funding: This research was supported by the Science and Technology Facilities Council of UK Joint Program Project (No. 61661136006002), National Nature Science Foundation (41801245), China Post-doctoral Foundation (No. 2017M620500), National Nature Science Foundation (41771371), GF Major Project (11-Y20A16-9001-17/18) and Science and Technology Facilities Council of UK- Newton AgriTech Programme (Project No. ST/N006798/1).

Acknowledgments: The authors acknowledge Juan Sui and Gongqi Zhou for providing the winter wheat yield data, which were used in this analysis.

Conflicts of Interest: The authors declare no conflicts of interest.

References

1. Sands, R.D.; Jones, C.A.; Marshall, E. Global Drivers of Agricultural Demand and Supply. Economic Research Report 186137, 2014. Available online: https://www.ers.usda.gov/webdocs/publications/45272/49035_err174.pdf?v=41900 (accessed on 16 October 2018).
2. Reynolds, M.; Tattaris, M.; Cossani, C.M.; Ellis, M.; Yamaguchi-Shinozaki, K.; Pierre, C.S. Exploring Genetic Resources to Increase Adaptation of Wheat to Climate Change. In *Advances in Wheat Genetics: From Genome to Field*; Ogiwara, Y., Takumi, S., Handa, H., Eds.; Springer: Tokyo, Japan, 2015.
3. Lesk, C.; Rowhani, P.; Ramankutty, N. Influence of extreme weather disasters on global crop production. *Nature* **2016**, *529*, 84–87. [[CrossRef](#)] [[PubMed](#)]
4. Gerighausen, H.; Lilienthal, H.; Jarmer, T.; Siegmann, B. Evaluation of Leaf Area Index and Dry Matter Predictions for Crop Growth Modelling and Yield Estimation. *EARSeL eProceedings* **2015**, 71–90. [[CrossRef](#)]
5. Atzberger, C. Advances in remote sensing of agriculture: Context description, existing operational monitoring systems and major information needs. *Remote Sens.* **2013**, *5*, 949–981. [[CrossRef](#)]
6. Jin, X.; Kumar, L.; Li, Z.; Xu, X.; Yang, G.; Wang, J. Estimation of winter wheat biomass and yield by combining the aquacrop model and field hyperspectral data. *Remote Sens.* **2016**, *8*, 972. [[CrossRef](#)]
7. Mulla, D.J. Twenty five years of remote sensing in precision agriculture: Key advances and remaining knowledge gaps. *Biosyst. Eng.* **2013**, *114*, 358–371. [[CrossRef](#)]
8. Casa, R.; Rossi, M.; Sappa, G.; Trotta, A. Assessing crop water demand by remote sensing and GIS for the Pontina Plain, Central Italy. *Water Resour. Manag.* **2009**, *23*, 1685–1712. [[CrossRef](#)]
9. Pourreza, A.; Lee, W.S.; Combs, R.; Roberts, P.; Ritenour, M. Spectral band selection to design a low cost sensor for citrus black spot disease detection. In Proceedings of the 2015 ASABE International Meeting, New Orleans, LA, USA, 26–29 July 2015; Volume 7004.
10. Yao, F.; Tang, Y.; Wang, P.; Zhang, J. Estimation of maize yield by using a process-based model and remote sensing data in the Northeast China Plain. *Phys. Chem. Earth* **2015**, *87–88*, 142–152. [[CrossRef](#)]
11. Moriondo, M.; Maselli, F.; Bindi, M. A simple model of regional wheat yield based on NDVI data. *Eur. J. Agron.* **2007**, *26*, 266–274. [[CrossRef](#)]
12. Prasad, A.K.; Chai, L.; Singh, R.P.; Kafatos, M. Crop yield estimation model for Iowa using remote sensing and surface parameters. *Int. J. Appl. Earth Obs. Geoinf.* **2006**, *8*, 26–33. [[CrossRef](#)]
13. Wu, Q.; Qi, B.; Zhao, T.; Yao, X.; Zhu, Y.; Gai, J. A Tentative Study on Utilization of Canopy Hyperspectral Reflectance to Estimate Canopy Growth and Seed Yield in Soybean. *Acta Agron. Sin.* **2013**, *39*, 309–318. [[CrossRef](#)]
14. Wu, J.; Sun, L.; Li, S.; Feng, R.; Ji, R.; Yu, W.; Zhang, Y. Correlation Analysis Between Hyperspectral Characteristics and Yield Components of Maize Under Low Temperature Stress. *Chin. Agric. Sci. Bull.* **2015**, *31*, 33–37.
15. Sid'ko, A.F.; Botvich, I.Y.; Pisman, T.I.; Shevyrnogov, A.P. Estimation of chlorophyll content and yield of wheat crops from reflectance spectra obtained by ground-based remote measurements. *Field Crops Res.* **2017**, *207*, 24–29. [[CrossRef](#)]
16. Sid'ko, A.F.; Botvich, I.Y.; Pisman, T.I.; Shevyrnogov, A.P. Estimation of the chlorophyll content and yield of grain crops via their chlorophyll potential. *Biophysics* **2017**, *62*, 456–459. [[CrossRef](#)]
17. Fang, H.; Liang, S.; Hoogenboom, G. Integration of MODIS LAI and vegetation index products with the CSM-CERES-Maize model for corn yield estimation. *Int. J. Remote Sens.* **2011**, *32*, 1039–1065. [[CrossRef](#)]

18. Dong, T.; Liu, J.; Qian, B.; Zhao, T.; Jing, Q.; Geng, X.; Wang, J.; Huffman, T.; Shang, J. Estimating winter wheat biomass by assimilating leaf area index derived from fusion of Landsat-8 and MODIS data. *Int. J. Appl. Earth Obs. Geoinf.* **2016**, *49*, 63–74. [[CrossRef](#)]
19. Tripathy, R.; Chaudhari, K.N.; Mukherjee, J.; Ray, S.S.; Patel, N.K.; Panigrahy, S.; Singh Parihar, J. Forecasting wheat yield in Punjab state of India by combining crop simulation model WOFOST and remotely sensed inputs. *Remote Sens. Lett.* **2013**, *4*, 19–28. [[CrossRef](#)]
20. Morel, J.; Bégué, A.; Todoroff, P.; Martiné, J.F.; Lebourgeois, V.; Petit, M. Coupling a sugarcane crop model with the remotely sensed time series of fIPAR to optimise the yield estimation. *Eur. J. Agron.* **2014**, *61*, 60–68. [[CrossRef](#)]
21. Morel, J.; Martiné, J.F.; Bégué, A.; Todoroff, P.; Petit, M. A comparison of two coupling methods for improving a sugarcane model yield estimation with a NDVI-derived variable. In Proceedings of the SPIE—The International Society for Optical Engineering, Edinburgh, UK, 24–27 September 2012; Volume 8531.
22. Huang, J.; Tian, L.; Liang, S.; Ma, H.; Becker-Reshef, I.; Huang, Y.; Su, W.; Zhang, X.; Zhu, D.; Wu, W. Improving winter wheat yield estimation by assimilating the leaf area index from Landsat TM and MODIS data into the WOFOST model. *Agric. For. Meteorol.* **2015**, *204*, 106–121. [[CrossRef](#)]
23. Huang, J.; Ma, H.; Su, W.; Zhang, X.; Huang, Y.; Fan, J.; Wu, W. Jointly Assimilating MODIS LAI and et Products into the SWAP Model for Winter Wheat Yield Estimation. *IEEE J. Sel. Top. Appl. Earth Obs. Remote Sens.* **2015**, *8*, 4060–4071. [[CrossRef](#)]
24. Huang, J.; Sedano, F.; Huang, Y.; Ma, H.; Li, X.; Liang, S.; Tian, L.; Zhang, X.; Fan, J.; Wu, W. Assimilating a synthetic Kalman filter leaf area index series into the WOFOST model to improve regional winter wheat yield estimation. *Agric. For. Meteorol.* **2016**, *216*, 188–202. [[CrossRef](#)]
25. Huang, J.; Ma, H.; Sedano, F.; Lewis, P.; Liang, S.; Wu, Q.; Su, W.; Zhang, X.; Zhu, D. Evaluation of regional estimates of winter wheat yield by assimilating three remotely sensed reflectance datasets into the coupled WOFOST–PROSAIL model. *Eur. J. Agron.* **2019**, *102*, 1–13. [[CrossRef](#)]
26. Igne, B.; Reeves, J.B.; McCarty, G.; Hively, W.D.; Lundc, E.; Hurburgh, C.R. Evaluation of spectral pretreatments, partial least squares, least squares support vector machines and locally weighted regression for quantitative spectroscopic analysis of soils. *J. Near Infrared Spectrosc.* **2010**, *18*, 167–176. [[CrossRef](#)]
27. Wahabzada, M.; Mahlein, A.K.; Bauckhage, C.; Steiner, U.; Oerke, E.C.; Kersting, K. Plant Phenotyping using Probabilistic Topic Models: Uncovering the Hyperspectral Language of Plants. *Sci. Rep.* **2016**, *6*, 1–11. [[CrossRef](#)] [[PubMed](#)]
28. Sytar, O.; Brestic, M.; Zivcak, M.; Olsovska, K.; Kovar, M.; Shao, H.; He, X. Applying hyperspectral imaging to explore natural plant diversity towards improving salt stress tolerance. *Sci. Total Environ.* **2017**, *578*, 90–99. [[CrossRef](#)] [[PubMed](#)]
29. Thenkabail, P.; Lyon, J.; Huete, A. (Eds.) Hyperspectral Indices and Image Classifications for Agriculture and Vegetation. 2018. Available online: https://books.google.com.hk/books?hl=zh-TW&lr=&id=HGR8DwAAQBAJ&oi=fnd&pg=PT9&dq=Hyperspectral+Indices+and+Image+Classifications+for+Agriculture+and+Vegetation&ots=zb5Onefn_A&sig=Ez626UZOXc1MZ8TVZYwYf6QBV8g&redir_esc=y#v=onepage&q=Hyperspectral%20Indices%20and%20Image%20Classifications%20for%20Agriculture%20and%20Vegetation&f=false (accessed on 16 October 2018).
30. Foster, A.J.; Kakani, V.G.; Mosali, J. Estimation of bioenergy crop yield and N status by hyperspectral canopy reflectance and partial least square regression. *Precis. Agric.* **2017**, *18*, 192–209. [[CrossRef](#)]
31. Fu, Y.; Yang, G.; Wang, J.; Song, X.; Feng, H. Winter wheat biomass estimation based on spectral indices, band depth analysis and partial least squares regression using hyperspectral measurements. *Comput. Electron. Agric.* **2014**, *100*, 51–59. [[CrossRef](#)]
32. Aguater, F.M.; Trachsel, S.; González Pérez, L.; Burgueño, J.; Crossa, J.; Balzarini, M.; Gouache, D.; Bogard, M.; de los Campos, G. Use of hyperspectral image data outperforms vegetation indices in prediction of maize yield. *Crop Sci.* **2017**, *57*, 2517–2524. [[CrossRef](#)]
33. Thorp, K.R.; Wang, G.; Bronson, K.F.; Badaruddin, M.; Mon, J. Hyperspectral data mining to identify relevant canopy spectral features for estimating durum wheat growth, nitrogen status, and grain yield. *Comput. Electron. Agric.* **2017**, *136*, 1–12. [[CrossRef](#)]

34. Rodrigues, F.A.; Blasch, G.; Defourny, P.; Ortiz-Monasterio, J.I.; Schulthess, U.; Zarco-Tejada, P.J.; Taylor, J.A.; Gérard, B. Multi-temporal and spectral analysis of high-resolution hyperspectral airborne imagery for precision agriculture: Assessment of wheat grain yield and grain protein content. *Remote Sens.* **2018**, *10*. [[CrossRef](#)]
35. Sui, J.; Qin, Q.; Ren, H.; Sun, Y.; Zhang, T.; Wang, J.; Gong, S. Winter wheat production estimation based on environmental stress factors from satellite observations. *Remote Sens.* **2018**, *10*. [[CrossRef](#)]
36. Wu, K.; Huang, R. The sustainable evaluations, the development potentialities and the countermeasures of water and land resources use in the Huang-Huai-Hai plain. *Sci. Geogr. Sin.* **2001**, *5*, 390–395. [[CrossRef](#)]
37. Jiang, Z.; Chen, Z.; Chen, J.; Liu, J.; Ren, J.; Li, Z.; Sun, L.; Li, H. Application of Crop Model Data Assimilation with a Particle Filter for Estimating Regional Winter Wheat Yields. *IEEE J. Sel. Top. Appl. Earth Obs. Remote Sens.* **2014**, *7*, 4422–4431. [[CrossRef](#)]
38. Zhang, Y.; Zheng, L.; Li, M.; Deng, X.; Ji, R. Predicting apple sugar content based on spectral characteristics of apple tree leaf in different phenological phases. *Comput. Electron. Agric.* **2015**, *112*, 20–27. [[CrossRef](#)]
39. Zhou, Q.; Li, J.; Liu, J.; Huang, H.; Sun, S. Two Dimensional correlation infrared spectroscopy of standard and false dahuang. *Chin. J. Anal. Chem.* **2003**, *31*, 1058–1061.
40. Noda, I. Vibrational two-dimensional correlation spectroscopy (2DCOS) study of proteins. *Spectrochim. Acta Part A Mol. Biomol. Spectrosc.* **2017**, *187*, 119–129. [[CrossRef](#)] [[PubMed](#)]
41. Qu, L.; Chen, J.; Zhou, Q.; Zhang, G.; Sun, S.; Guo, Y. Identification of authentic and adulterated *Aquilaria Lignum Resinatum* by Fourier transform infrared (FT-IR) spectroscopy and two-dimensional correlation analysis. *J. Mol. Struct.* **2016**, *1124*, 216–220. [[CrossRef](#)]
42. Battiti, R. Using Mutual Information for Selecting Features in Supervised Neural Net Learning. *IEEE Trans. Neural Netw.* **1994**, *5*, 537–550. [[CrossRef](#)]
43. Lewis, D.D. Feature Selection and Feature Extraction for Text Categorization. In Proceedings of the Workshop on Speech and Natural Language, Harriman, NY, USA, 23–26 February 1992; Association for Computational Linguistics: Chicago, IL, USA, 1992; pp. 212–217.
44. Benoudjit, N.; François, D.; Meurens, M.; Verleysen, M. Spectrophotometric variable selection by mutual information. *Chemom. Intell. Lab. Syst.* **2004**, *74*, 243–251. [[CrossRef](#)]
45. Hu, Q.; Zhang, L.; Zhang, D.; Pan, W.; An, S.; Pedrycz, W. Measuring relevance between discrete and continuous features based on neighborhood mutual information. *Expert Syst. Appl.* **2011**, *38*, 10737–10750. [[CrossRef](#)]
46. Viscarra Rossel, R.A.; Walvoort, D.J.J.; McBratney, A.B.; Janik, L.J.; Skjemstad, J.O. Visible, near infrared, mid infrared or combined diffuse reflectance spectroscopy for simultaneous assessment of various soil properties. *Geoderma* **2006**, *131*, 59–75. [[CrossRef](#)]
47. Cortes, C.; Vapnik, V. Support-Vector Networks. *Mach. Learn.* **1995**, *20*, 273–297. [[CrossRef](#)]
48. Cristianini, N.; Shawe-Taylor, J. *An Introduction to Support Vector Machines and Other Kernel-Based Learning Methods*; Cambridge University Press: Cambridge, UK, 2000.
49. Yuan, H.; Yang, G.; Li, C.; Wang, Y.; Liu, J.; Yu, H.; Feng, H.; Xu, B.; Zhao, X.; Yang, X. Retrieving soybean leaf area index from unmanned aerial vehicle hyperspectral remote sensing: Analysis of RF, ANN, and SVM regression models. *Remote Sens.* **2017**, *9*, 309. [[CrossRef](#)]
50. Verrelst, J.; Muñoz, J.; Alonso, L.; Delegido, J.; Rivera, J.P.; Camps-Valls, G.; Moreno, J. Machine learning regression algorithms for biophysical parameter retrieval: Opportunities for Sentinel-2 and -3. *Remote Sens. Environ.* **2012**, *118*, 127–139. [[CrossRef](#)]
51. Chang, C.; Lin, C. Libsvm: A Library for Support Vector Machines. *ACM Trans. Intell. Syst. Technol.* **2011**, *2*, 1–27. [[CrossRef](#)]
52. Datt, B. Remote Sensing of Chlorophyll a, Chlorophyll b, Chlorophyll a+b, and Total Carotenoid Content in Eucalyptus Leaves. *Remote Sens. Environ.* **1998**, *66*, 111–121. [[CrossRef](#)]
53. Acevedo, E.; Silva, P.; Silva, H. Wheat growth and physiology. In *Bread Wheat Improvement and Production*; FAO: Rome, Italy, 2002; Volume 30.
54. Zhao, D.; Raja Reddy, K.; Kakani, V.G.; Read, J.J.; Carter, G.A. Corn (*Zea mays* L.) growth, leaf pigment concentration, photosynthesis and leaf hyperspectral reflectance properties as affected by nitrogen supply. *Plant Soil* **2003**, *257*, 205–217. [[CrossRef](#)]
55. Daigger, L.; Sander, D.; Peterson, G. Nitrogen content of winter wheat during growth and maturation. *Agron. J.* **1976**, *68*, 815–818. [[CrossRef](#)]

56. Buchwald, H.E.; Wolff, C. Further Evidence for Carotenoids Engaged in a Metastable State in Photosynthesis. *Zeitschrift für Naturforschung B* **1971**, *26*, 51–53. [[CrossRef](#)]
57. Rise, M.; Cojocar, M.; Gottlieb, H.E.; Goldschmidt, E.E. Accumulation of α -tocopherol in senescing organs as related to chlorophyll degradation. *Plant Physiol.* **1989**, *89*, 1028–1030. [[CrossRef](#)]
58. Li, M.Z. *Spectral Analysis Technique and Its Application*; Science Press: Beijing, China, 2006.
59. Poorani, T.R.; Vellingiria, V.; Deepa, V.S.; Abdula, A.N. Formulation of Eichhornia Crassippes Derived Lutein: Coconut Oil Micro-Emulsion for Sustained Ophthalmic Drug Delivery. *Int. J. Pharm. Sci. Res.* **2017**, *8*, 4159–4171. [[CrossRef](#)]
60. Sewe, K.U.; Reich, R. The Effect of Molecular Polarization on the Electrochromism of Carotenoids: II. Lutein-Chlorophyll Complexes: The Origin of the Field-Indicating Absorption-Change at 520 nm in the Membranes of Photosynthesis. *Zeitschrift für Naturforschung C* **1977**, *32*, 161–171. [[CrossRef](#)]
61. Zhao, D.; Reddy, K.R.; Kakani, V.G.; Reddy, V.R. Nitrogen deficiency effects on plant growth, leaf photosynthesis, and hyperspectral reflectance properties of sorghum. *Eur. J. Agron.* **2005**, *22*, 391–403. [[CrossRef](#)]
62. An, J. Effect of Lighe and Spectrum on Hydrogen Production Technics by Photosynthetic Bacteria. Master's Thesis, Henan Agricultural University, Zhengzhou, China, 2009.
63. Gao, J.; Li, P.; Ma, F.; Goltsev, V. Photosynthetic performance during leaf expansion in *Malus micromalus* probed by chlorophyll a fluorescence and modulated 820 nm reflection. *J. Photochem. Photobiol. B Biol.* **2014**, *137*, 144–150. [[CrossRef](#)] [[PubMed](#)]
64. Verrelst, J.; Rivera, J.P.; Moreno, J. ARTMO's Global Sensitivity Analysis (GSA) Toolbox to Quantify Driving Variables of Leaf and Canopy Radiative Transfer Models. *EARSeL eProceedings* **2015**, 1–11. [[CrossRef](#)]
65. Fischer, R.A. Wheat. In *Potential Productivity of Field Crops under Different Environments*; International Rice Research Institute: Los Baños Laguna, Philippines, 1983; pp. 129–154.
66. Parry, M.A.J.; Reynolds, M.; Salvucci, M.E.; Raines, C.; Andralojc, P.J.; Zhu, X.G.; Price, G.D.; Condon, A.G.; Furbank, R.T. Raising yield potential of wheat. II. Increasing photosynthetic capacity and efficiency. *J. Exp. Bot.* **2011**, *62*, 453–467. [[CrossRef](#)]
67. Ainsworth, E.A.; Long, S.P. What have we learned from 15 years of free-air CO₂ enrichment (FACE)? A meta-analytic review of the responses of photosynthesis, canopy properties and plant production to rising CO₂. *New Phytol.* **2005**, *165*, 351–372. [[CrossRef](#)]
68. Lin, F.; Ding, X.; Fu, Z.; Deng, J.; Shen, Z. Application of mutual information to variable selection in diagnosis of phosphorus nutrition in rice. *Spectrosc. Spectr. Anal.* **2009**, *29*, 2467–2470.
69. Read, J.J.; Tarpley, L.; McKinion, J.M.; Reddy, K.R. Narrow-Waveband Reflectance Ratios for Remote Estimation of Nitrogen Status in Cotton. *J. Environ. Qual.* **2002**, *31*, 1442. [[CrossRef](#)]
70. Gómez-Sanchis, J.; Martín-Guerrero, J.D.; Soria-Olivas, E.; Martínez-Sober, M.; Magdalena-Benedito, R.; Blasco, J. Detecting rottenness caused by *Penicillium* genus fungi in citrus fruits using machine learning techniques. *Expert Syst. Appl.* **2012**, *39*, 780–785. [[CrossRef](#)]
71. Ververis, C.; Georghiou, K.; Danielidis, D.; Hatzinikolaou, D.G.; Santas, P.; Santas, R.; Corleti, V. Cellulose, hemicelluloses, lignin and ash content of some organic materials and their suitability for use as paper pulp supplements. *Bioresour. Technol.* **2007**, *98*, 296–301. [[CrossRef](#)]
72. Johkan, M.; Shoji, K.; Goto, F.; Hahida, S.; Yoshihara, T. Effect of green light wavelength and intensity on photomorphogenesis and photosynthesis in *Lactuca sativa*. *Environ. Exp. Bot.* **2012**, *75*, 128–133. [[CrossRef](#)]
73. Kinoshita, T.; Doi, M.; Suetsugu, N.; Kagawa, T.; Wada, M.; Shimazaki, K. Phot1 and phot2 mediate blue light Regulation of Stomatal Opening. *Nature* **2001**, *414*, 656–660. [[CrossRef](#)] [[PubMed](#)]
74. Takemiya, A.; Inoue, S.; Doi, M.; Kinoshita, T.; Shimazaki, K. Phototropins promote plant growth in response to blue light in low light environments. *Plant Cell* **2005**, *17*, 1120–1127. [[CrossRef](#)]
75. Yao, X.; Zhu, Y.; Tian, Y.C.; Feng, W.; Cao, W.X. Exploring hyperspectral bands and estimation indices for leaf nitrogen accumulation in wheat. *Int. J. Appl. Earth Obs. Geoinf.* **2010**, *12*, 89–100. [[CrossRef](#)]
76. Gitelson, A.A.; Merzlyak, M.N. Signature analysis of leaf reflectance spectra: Algorithm development for remote sensing of chlorophyll. *J. Plant Physiol.* **1996**, *148*, 494–500. [[CrossRef](#)]

